THE TIME-OF-FLIGHT ENERGY, ANGLE, MASS SPECTROGRAPH (TEAMS) EXPERIMENT FOR FAST

D. M. KLUMPAR, E. HERTZBERG, W. K. PETERSON, and E. G. SHELLEY
Lockheed Martin, Advanced Technology Center, Palo Alto, CA 94304-1191

E. MÖBIUS, L. M. KISTLER, M. POPECKI, K. CROCKER, M. GRANOFF, and L. TANG
Institute for the Study of Earth, Oceans and Space,
University of New Hampshire, Durham, NH 03824

C. W. CARLSON and J. McFADDEN
Space Sciences Laboratory, University of California Berkeley, Berkeley, CA

B. KLECKER, F. EBERL, E. KÜNNETH, H. KÄSTLE, M. ERTL, and D. HOVESTADT
Max-Planck-Institut für extraterrestrische Physik, Garching, Germany

Abstract. The Time-of-flight Energy Angle Mass Spectrograph (TEAMS) is being flown on the FAST Small Explorer mission to measure the 3-dimensional distribution function of the major ion species present in the lower magnetosphere. The instrument is similar to time-of-flight plasma analyzer systems that have been designed and planned for flight as CODIF (COmposition and DIstribution Function analyzer) on the four European Space Agency Cluster-II spacecraft and, as ESIC (Equator-S Ion Composition instrument) on Equator-S. This instrument allows the 3-dimensional distribution functions of individual ion species to be determined within 1/2 spin period (2.5 sec). Two-dimensional distributions are measured in 80 msec. These capabilities are crucial for the study of selective energization processes in the auroral regions of the magnetosphere. The design, operational characteristics, and test and calibration results for this instrument are presented. The sensor consists of a toroidal top-hat electrostatic analyzer with instantaneous acceptance of ions over 360• in polar angle. After post-acceleration of the incoming ions by up to 25 kV, a time-of-flight mass spectrograph discriminates the individual species. It has been demonstrated through calibration that the instrument can easily separate H^+, He^{2+}, He^+, O^+ and, for energies after post-acceleration of > 20 keV, even O_2^+ molecules. On-board mass discrimination and the internal accumulation of several distinct data quantities combined with the spacecraft's flexible telemetry formatting allow for instrument data rates from 7.8 kb/sec to 315 kb/sec to be telemetered to ground through the FAST centralized Instrument Data Processor.

Table of Contents

1. Introduction

The early suborbital rocket and satellite investigations of the auroral region in the 1960s determined that precipitating electrons were the dominant contributor to auroral luminosity. As more in-depth investigations of auroral processes were carried out it was learned that ionospheric ions play a significant role in auroral electrodynamic processes.

Mass spectrometry performed in the magnetosphere revealed that a significant and variable component of the plasma population was of ionospheric origin (Shelley et al., 1972; Young et al., 1977). At high polar altitudes, above the auroral region, precipitating O^+ ions, necessarily of geogenic origin, were observed during a magnetic storm at energies in excess of 10 keV with intensities greater than the accompanying protons (Shelley et al., 1972). Direct measurement of outgoing accelerated ions using mass spectrometers at high altitudes were subsequently confirmed by Shelley et al. (1976), and by Sharp et al. (1977); and with non-mass-resolving ion analyzers at low altitude (Klumpar, 1979), demonstrating the direct outflow of ionospheric ions. Physical processes were found to be active within and above the auroral ionosphere that result in the direct injection of ionospheric ions into the magnetosphere.

The broad objective of the Time-of-flight Energy Angle Mass Spectrograph (TEAMS) investigation on FAST is to directly characterize the three dimensional distributions of ions within these interaction regions, in order to understand the evolution of the ion distributions from cold ambient ionospheric plasma to hot accelerated magnetospheric particles and to discern the physical mechanisms that drive this evolution.

2. Instrument Heritage

Following the successful application of time-of-flight (TOF) mass-spectrographs in space pioneered with the AMPTE mission in 1984 (Gloeckler et al., 1985; McEntire et al., 1985; Möbius et al., 1985) TOF instruments have become a standard tool in space plasma physics. TOF instruments have been flown in various configurations on missions, such as VIKING, GIOTTO, VEGA, PHOBOS, Ulysses, and Cassini. They are also aboard the GGS spacecraft. The wealth of the ion composition results from these missions has clearly demonstrated the excellent capabilities of this type of instrumentation in both the energy range of the bulk plasma as well as in the energy gap between about 30 keV and several hundred keV/nucleon, which existed between the regimes of magnetic mass spectrographs and cosmic ray telescopes.

To simultaneously determine the 3-dimensional distribution function and the mass-composition of ions, the concept of the fast 3-D plasma instrument based on the top-hat design after Carlson et al. (1982) and first flown on AMPTE/ IRM (Paschmann et al., 1985) has been combined with the TOF technique and post-acceleration. A suite of similar instruments were designed for the ESA/NASA Cluster mission (Rème et al., 1993) as CODIF, for FAST as TEAMS, and for Equator-S as ESIC. For a description of this instrument family see Möbius et al. (1998b).

In this paper we describe the Time-of-Flight Energy Angle Mass Spectrograph (TEAMS) flown on the FAST Small Explorer Mission. The major achievement of this instrument will be to allow the accumulation of full 3-dimensional velocity distribution functions for four major species (e.g., H^+, He^{2+}, He^+ and O^+) within 1/2 spin period of the FAST spacecraft. The instantaneous coverage of a two-dimensional cut of the distribution function is possible within one energy sweep whose typical duration is 80-160 msec. This capability will significantly enhance our knowledge of the dynamics, heating and acceleration of multi-ion plasmas that are typical of the auroral region.

3. Instrument Description

The instrument combines the selection of incoming ions according to their energy per charge by electrostatic deflection in a toroidal analyzer with post-acceleration by up to 25 keV/e and subsequent time-of-flight analysis. A top view and a cross-sectional view of the sensor showing the basic principles of operation are presented in Fig. 1a. The instrument is mounted with its axis of symmetry perpendicular to the spacecraft spin axis. The front end of the sensor protrudes beyond the spacecraft surface so that its 360º aperture has a free field-of-view.

The instrument design and orientation complement the electrostatic analyzer (ESA) instrument package on FAST (Carlson et al., 1998, 2000) in two ways. First, TEAMS provides mass resolution capability, while the ESAs measure total ion flux without resolving mass, but with high time resolution. Second, TEAMS is oriented with the spin axis in the plane of its viewing field, allowing the full 3-dimensional velocity distribution of all ions to be measured in half a spin period. The FAST spin period is maintained at 5 seconds. TEAMS is the only fully 3-D particle sensor on FAST. The ESAs are oriented with their viewing field perpendicular to the spin axis and thus cover the full pitch-angle range at any instant. In this way the highest time resolution can be achieved.

3.1 SENSOR

The electrostatic analyzer (ESA) is a rotationally symmetric toroidal top-hat with a uniform response over 360º of polar angle. Toroidally symmetric electrostatic analyzers carry the advantage of an extended focal length in the polar direction as compared to spherical analyzers, allowing them to be matched to a following mass-resolving analyzer. Toroidal geometries have been been developed and used for space plasma analyzers in the past (e.g. Ghielmetti and Young, 1987, Young et al, 1988, Rème, 1993, Shelley et al., 1995). As illustrated in Figures 1a and 1b, the analyzer consists of an inner toroid, to which a variable negative potential is applied, an outer toroid with a cut-out at the top, and a top-cap lifted above the outer toroid. The analyzer carries a toroidal plate spacing of 4 mm. The inner and outer toroid radii are 61 mm and 65 mm, respectively, about a center of curvature displaced 12.1 mm from the rotational symmetry axis. The inner toroidal sections are bridged by a 17.9° hemispherical section of radius 100.4 mm centered on a point 37.5 mm below the center of curvature of the toroid. Along the centerline the top cap is elevated 12.73 mm above the inner spherical section. Both the outer toroid and the top-cap are held at ground potential, thereby exposing no high voltage to the external plasma. The outer toroid is scalloped to minimize the transparency to scattered ions and to reduce stray solar UV radiation. For the same reason the toroid surfaces are covered with a gold black coating. A beam of parallel ion trajectories entering the aperture is focused to a certain location at the exit plane of the analyzer. This location determines the incident polar angle of the ions. With an applied cross-plate voltage of 0.12 V to 1500 V (varied with 192 logarithmically spaced steps) incident ions with energies per charge from 1 eV/e to 12000 eV/e are selected. The analyzer has an intrinsic energy resolution of $\bullet E/E \sim 0.15$. It is surrounded by a cylindrical collimator which serves to define the acceptance angles. The full polar angle of the analyzer is divided into 16 pixels of 22.5º each. The full energy sweep is performed 32 times per spin (or 64 times per spin in high speed mode). Thus a two dimensional cut through the distribution function in polar angle with 11.25º (or 5.625º) sample spacing in azimuthal angle is obtained every 1/32 (or 1/64) of a spin period. The geometric factor for one individual pixel is $A \cdot \Delta E/E \cdot \Delta\theta \cdot \pi/8 \sim 1.5 \cdot 10^{-3}$ cm^2 sr, where A denotes the aperture area and $\Delta\theta$ the azimuthal width of the analyzer. This value takes into account the transmissivity of all grids and support structures in the sensor, but not the detection efficiency which varies with species and energy and will be discussed later.

Behind the energy per charge analyzer the ions are accelerated by a selectable post-acceleration voltage of -15 to -25 kV, such that the ions have at least an energy of 15 keV/e before entering the TOF-section. The energy per charge E/Q as selected by the electrostatic analyzer plus the energy $e \cdot U_{ACC}$ gained by post-acceleration are combined with the measured

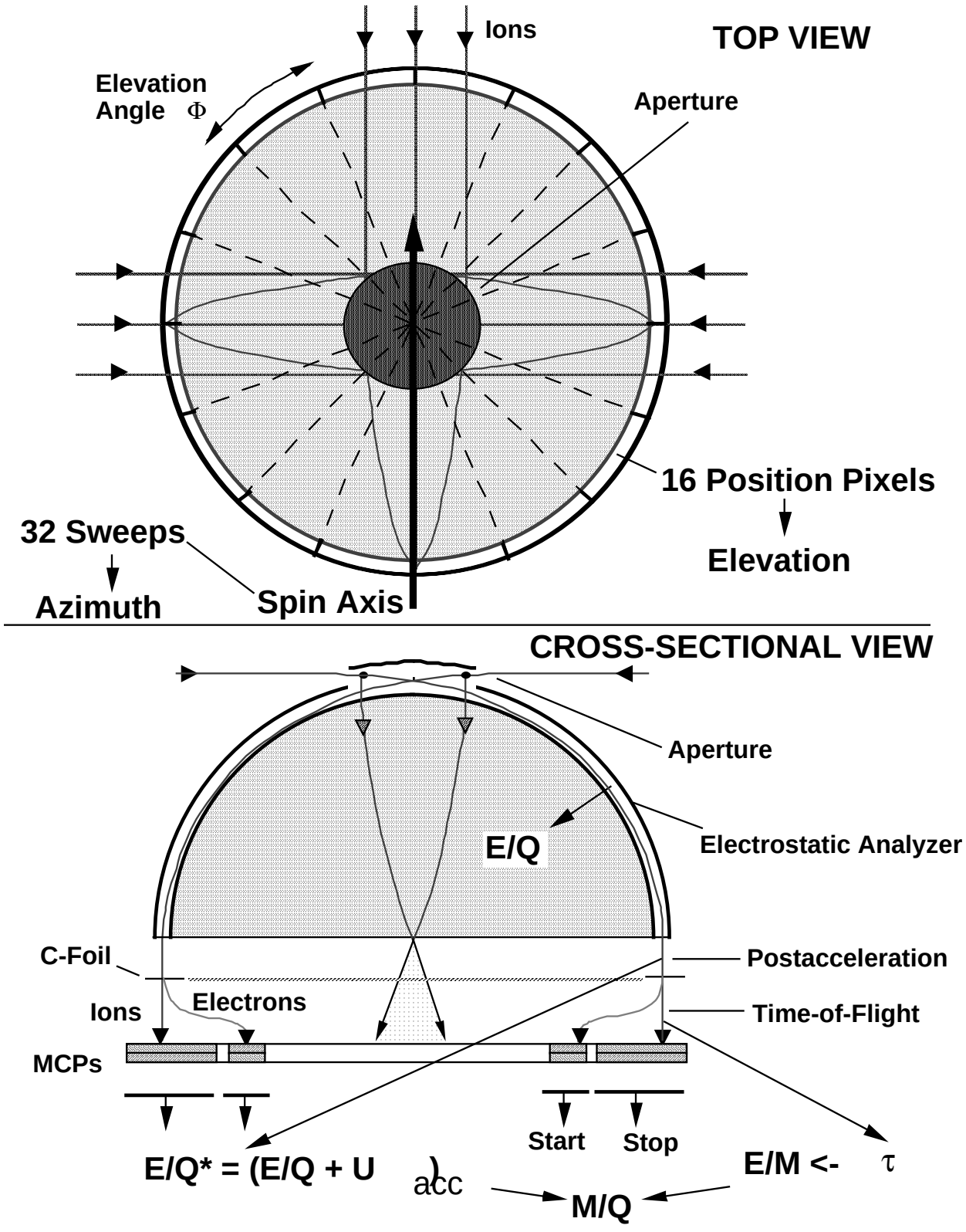

Fig. 1a.. Schematic top and cross-sectional views of sensor showing principles of operation.

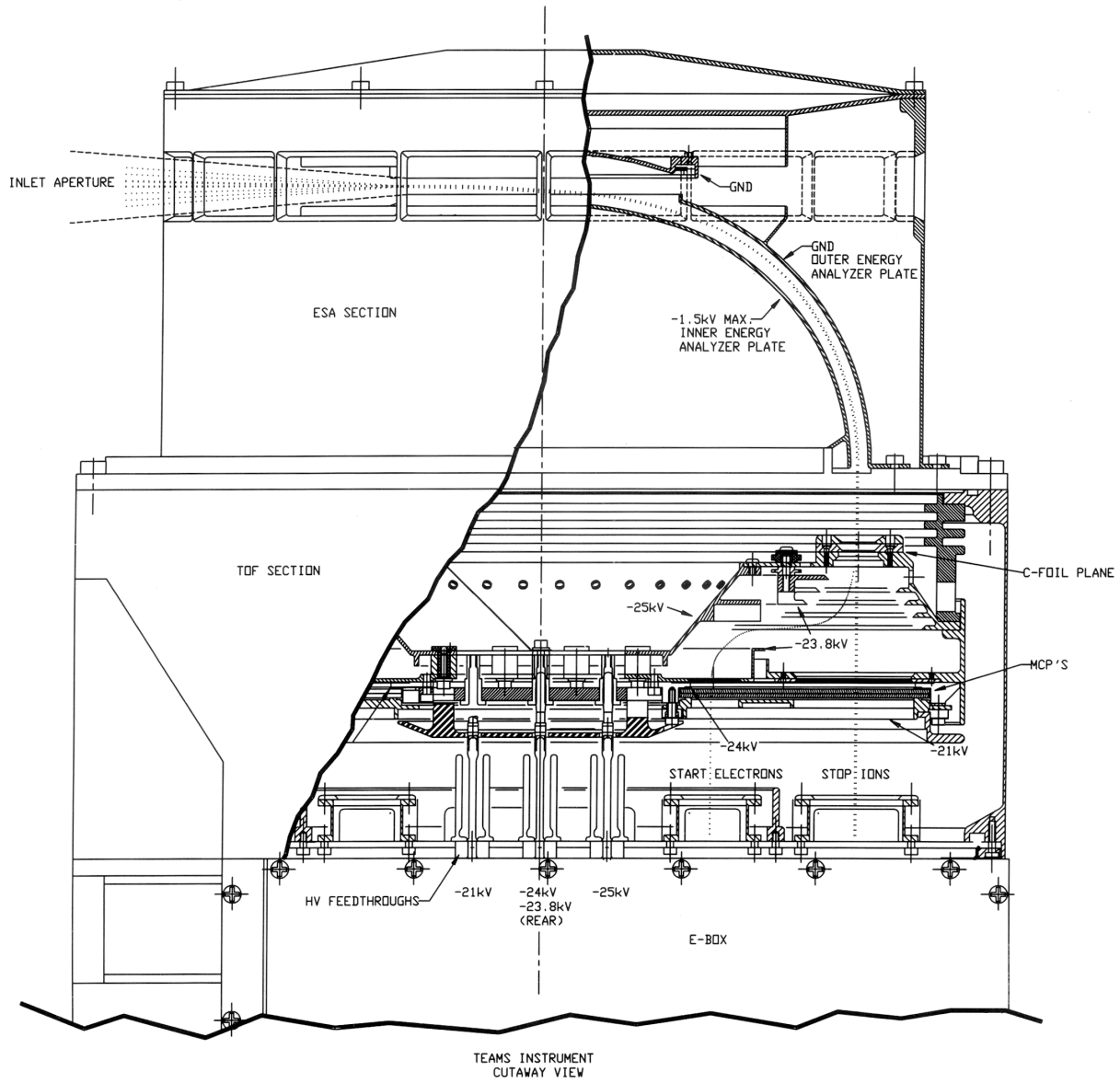

Fig. 1b.. TEAMS ion optics elements in cut-away view showing potential surfaces.

time-of-flight τ through the length d of the time-of-flight (TOF) unit to give the mass per charge M/Q of the ion according to:

$$M/Q = 2(E/Q + e \cdot U_{ACC} - E_{loss})/(d/\tau)^2 .$$

The quantity E_{loss} represents the effect of energy loss in the thin carbon foil (~ 3μg/cm^2) at the entry of the TOF section and depends on particle species and incident energy. The flight path of the ions is defined by the 3 cm distance between the carbon foil at the entrance and the surface of the stop microchannel plate (MCP). The Start signal is provided by secondary electrons, that are emitted from the carbon foil during the passage of the ions. The electrons are accelerated and deflected onto the start portion of the MCP by the appropriate potential configuration (e.g. Figure 1b). The secondary electrons also provide the position information for the angular sectoring. To allow good angular resolution, a toroidal geometry has been chosen for the analyzer which pushes its focal point close to the carbon foil plane. The carbon foil is made up of 22.5º sectors, separated by narrow metal strips. The electron optics are designed to strongly

focus secondary electrons originating at a foil onto the corresponding MCP start sector, using the fringe fields of the radial foil support structures and radial fin separators between the sectors. The MCP assemblies are ring shaped quadrants with radii of 3 by 9 cm (inner and outer radii, respectively) which serve both the start and stop signals.

The electron clouds exiting the MCPs are accelerated by the negative postacceleration potential to the signal pickup assemblies which are at ground potential. The signal assemblies consist of two sets of thin wire grids with • 85% transmission at a distance of 10 mm in front of a segmented signal plate. The timing information is taken from the grids, separately for two 180º segments. The position of the incoming ions is taken from sixteen 22.5º signal plate pixels behind the start section of the MCPs complemented by four 90º pixels behind their stop section. In this way the timing and position signals are electrically separated already at the source of the signal.

3.2 SENSOR ELECTRONICS

The sensor electronics consists of two time-to-amplitude converters (TACs) to measure the time-of-flight of the ions separately for two halves of the TOF section, sixteen position discriminators at the start and four position discriminators at the stop section of the MCPs, as well as event selection logic. A schematic block diagram is shown in Figure 2. A valid ion event requires the basic coincidence of a start and stop signal as well as the simultaneous registration of a start and stop position signal in the matching quadrant. In addition, only one start position at a time may be triggered. This configuration constitutes the normal operation mode. Via telecommand the requirements can be loosened by dropping the quadrant matching requirement. In addition the raw pulse height data can be configured to include events with multiple starts, mainly for diagnostic purposes. Each individual ion event is pulse height analyzed according to its time-of-flight, incidence in azimuthal (given by the spacecraft spin) and polar angle (given by the start position), and the energy per charge (given by the actual deflection voltage). In addition, counters accumulate rates individually for each start and position signal as well as for all time-of-flight measurements, all events with multiple start positions, events with only a single start position, and events that fall below a preset time-of-flight.

The postacceleration voltage is provided by a DC-DC converter with a 12 stage multiplier. The voltage can be set to voltages up to -25 kV via telecommand. The MCP bias voltage is supplied by a converter with a similar design, whose high voltage multiplier stages are referenced to the second-last stage of the postacceleration multiplier. The MCP voltage can be commanded up to 4 kV, thus providing adequate margin to compensate for potential gain degradation of the MCPs during the mission. The normal operating voltage is about 3 kV. The high voltage circuitry is protected by a current-sensitive circuit that turns the corresponding supply off upon detection of a discharge. The voltages and currents of all high voltage supplies are monitored by housekeeping ADCs along with the internal supply voltages of the sensor electronics and temperatures in the sensor, analog and digital electronics.

A detailed discussion of several critical design aspects of this instrument may be found in Möbius et al., 1998b.

4. TEAMS Interface to FAST Instrument Data Processing Unit

The instrument includes a hardware signal processing unit that compresses the original pulse height information and handles the sensor control functions and housekeeping data collection.

4.1 DATA COMPRESSION

To compress the data, look-up tables are stored on board which give the mass/charge bin, given the time-of-flight and energy/charge and the solid angle bin, given the input polar angle and azimuthal (spin) angle. Based on a comparison with these look-up tables each valid event is

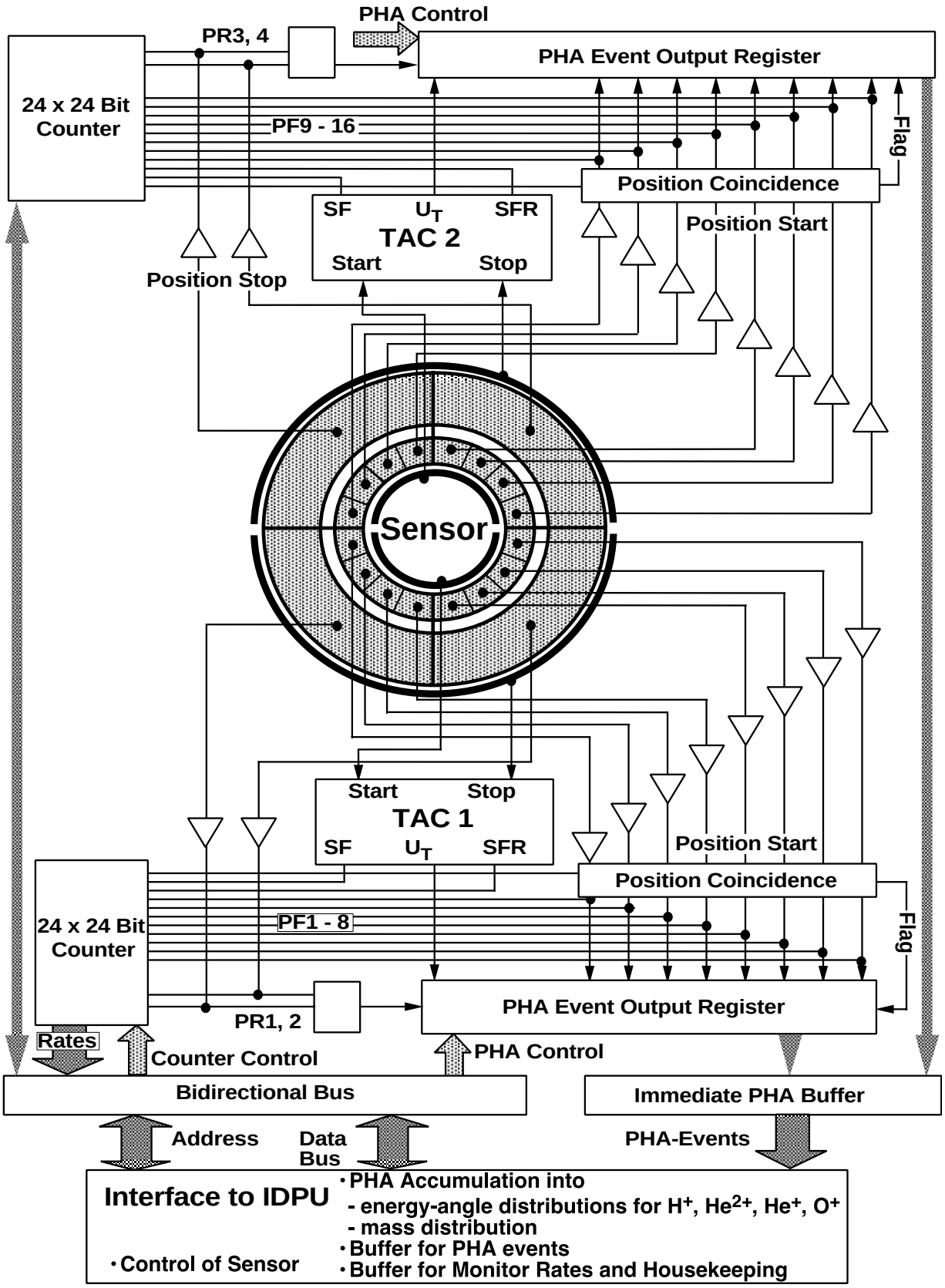

Fig. 2. Sensor electronics block diagram.

accumulated into incrementing memories; one with 48 energy bins, 64 solid angle bins, and 4 mass bins, and a separate memory with 16 energy, 16 solid angle, and 64 mass bins. While the first accumulator is designed to support detailed high time resolution studies of the velocity distributions of the 4 major species, the second one allows a more detailed composition study with longer accumulation times. In parallel, the events are also accumulated into a 4 species burst accumulator with the full resolution in azimuthal and elevation angle, whose contents is transmitted in conjunction with other high speed data products of the payload upon specially set trigger conditions. A separate memory allocation is set aside to accumulate high time resolution data for four species from the two pairs of angle sectors that lie adjacent to the spin axis. The resulting data products: survey, hi-mass, burst and pole data are described in more detail below. Because the mass/charge algorithm depends on the total energy of the ion (incoming energy plus post-acceleration), a new mass table must be loaded when the post-acceleration voltage is changed. The ability to upload new tables also allows flexibility in choosing the 4 species used in the survey, burst and pole data products.

In addition, a sample of raw pulse height events, monitor rates, and status data are taken and stored in a separate memory block. The memory blocks are read out by the centralized Instrument Data Processing Unit (IDPU) in 1 kB blocks. Rotating buffering of the memory assures the integrity of the data during readout.

4.2 INSTRUMENT COMMAND AND CONTROL

The interface board also contains the command registers and high voltage control circuits. Both the postacceleration and MCP supplies are controlled by 8 bit DACs via telecommand. The sweep supply for the analyzer is controlled by a 16 bit DAC whose LSB is ignored. The sweep is performed from a sweep table in the ACTEL logic synchronized with the instrument clock and the spin phase. All HV supplies require an enable command in addition to a setting > 0.

When the payload is not taking data, TEAMS is placed in a low-power standby mode with only the interface electronics and the postacceleration supply powered. The instrument is brought into its fully operational condition by turning on in sequence the accumulator electronics, the sensor electronics and ramping up the MCP bias voltage to its operational value. The two time-of-flight circuits and related position amplifiers can be powered separately.

The upload of mass and angle look-up tables requires the instrument in a condition with only the digital accumulator electronics on. Simultaneous sensor signals would disrupt the memory write operations.

An Inflight Calibration circuit allows the stimulation of both the time-to-amplitude converters and the position amplifiers with simulated events, whose time-of-flight can be varied by a DAC. A predefined calibration sequence will be run every few weeks over the course of the mission to monitor the performance of the analog and digital electronics independently of the sensor performance.

5. Data Products and Instrument Modes

The TEAMS instrument produces five science data products. Two additional data products (monitor rates and status) provide instrument operational information at a basic level. Internally all data products are being produced and accumulated continuously. The payload telemetry mode determines which one or which combination of data products are read by the FAST IDPU and placed into the FAST data stream. In addition rates data are always telemetered, as an engineering monitor. The five science data products are: burst, survey, pole, high mass resolution (hi-mass), and PHA as described below:

5.1 DATA PRODUCTS

5.1.1 Burst

Burst data is full resolution data for four mass groups (normally H^+, O^+, He^+, and He^{++}). For each step of an energy sweep (48 major E-steps) data is collected from all sixteen position pixels. The 32 (or 64) azimuthal look directions are accumulated consecutively over a spin period. These data are not compressed. Burst data is read into the IDPU irrespective of TEAMS telemetry mode. Its presence in the telemetered data stream depends upon spacecraft telemetry mode. Burst data are contained in application identifier (APID) 1047 (hex 417) in the FAST telemetry stream.

5.1.2 Survey

Survey data is basically high resolution energy and angle data consisting of 4 mass groups, 48 energies, and 64 solid angle segments. The 4 mass groups selected are H^+, O^+, He^+, and He^{++}. The 64 solid angle segments (organized by spin phase) consist of 16 equatorial segments (combining the pixels that map into the same solid angle element after 1/2 spin, PF4+PF13 and PF5+PF12, respectively); 8 lower-mid-latitude, 4 upper-mid-latitude, and 4 polar segments in each hemisphere (see Fig 3a). The equatorial solid angle segments contain 2 (4) samples at each energy in the 32 (64) sweep/spin mode. Polar solid angle segments contain 8 and 16 samples at each energy for 32 and 64 sweep per spin modes respectively. The full angular range is covered in half a spin but the actual time resolution of the measurement depends upon the telemetry mode. In the highest telemetry rate modes H^+ and O^+ survey data come out every half spin. In lowest telemetry rate mode these data are accumulated for 4 spins. In every mode He^+ and He^{++} are accumulated twice as long as H^+ and O^+ before being read out. The data are compressed from two bytes to one byte in the IDPU. Survey data are contained in APID 1027 (hex 403).

5.1.3 Pole Data

This science data quantity consists of high time resolution data along the spin axis. Because the spin axis is oriented perpendicular to the magnetic field in the key operation region of the satellite, 90º pitch-angle particles are collected in the Pole data. Data is accumulated from each of the two pairs of angle sectors that straddle the spin axis (PF1 and PF16 receive ions moving along the spin axis direction and PF8 and PF9 receive ions moving in the negative z-axis direction). Only the upper 32 energy steps are used for this data product (26 eV to 12 keV). The same four standard mass groups are accumulated, however the selected telemetry mode determines which mass groups are placed into the telemetry stream (see Table II). The data are

Sweeps →

	1/4 Spin								1/2 Spin								3/4 Spin								1 Spin							
64 Sweeps	0	2	4	6	8	10	12	14	16	18	20	22	24	26	28	30	32	34	36	38	40	42	44	46	48	50	52	54	56	58	60	62
32 Sweeps	0	1	2	3	4	5	6	7	8	9	10	11	12	13	14	15	16	17	18	19	20	21	22	23	24	25	26	27	28	29	30	31
PF1	8								40								24								56							
PF2	9								41								25								57							
PF3	2				10				34				42				18				26				50				58			
PF4	0		3		6		11		32		35		38		43		16		19		22		27		48		51		54		59	
PF5	1		4		7		12		33		36		39		44		17		20		23		28		49		52		55		60	
PF6	5				13				37				45				21				29				53				61			
PF7	14								46								30								62							
PF8	15								47								31								63							
PF9	31								63								15								47							
PF10	30								62								14								46							
PF11	21				29				53				61				5				13				37				45			
PF12	17		20		23		28		49		52		55		60		1		4		7		12		33		36		39		44	
PF13	16		19		22		27		48		51		54		59		0		3		6		11		32		35		38		43	
PF14	18				26				50				58				2				10				34				42			
PF15	25								57								9								41							
PF16	24								56								8								40							
	(0-31)								(32-63)								(0-31)								(32-63)							

Fig. 3a. Solid angle map for survey data.

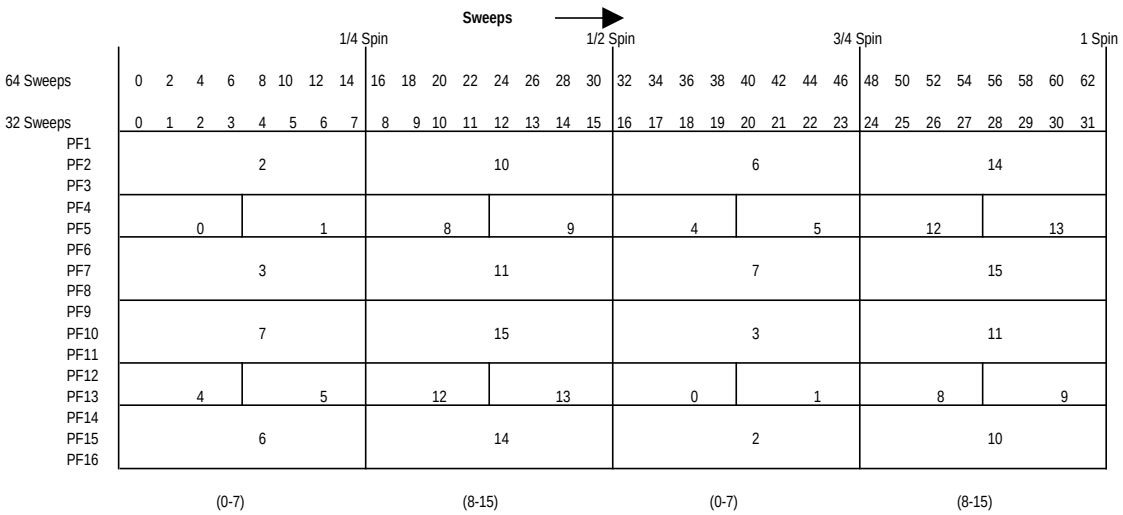

Fig. 3b. Solid angle map for HiMass data.

accumulated for 8 sweeps and therefore are read out every 1/4 spin for 32 sweep/spin modes and every 1/8th spin for 64 sweep/spin modes. Pole data are contained in APID 1029 (hex 405).

5.1.4 High Mass Resolution Data (hi-mass)

The primary purpose of the high mass resolution science data quantity is to collect mass spectra over the full mass response of the spectrograph at relatively low time and energy resolution. Data are accumulated into 64 mass, 16 energy, and 16 solid angle segments. This array is read out by the IDPU every 16 s/c spins (80 sec) for telemetry modes 0-3; every 8 s/c spins (40 sec) for modes 4 and 5; and every 4 s/c spins (20 sec) for modes 6 and 7. The mass bins cover from 0.6 to 60 AMU, in 64 logarithmically spaced steps. Each of the 16 energy bins is the sum of 3 adjacent major energy steps. The 16 solid angle segments cover the unit sphere as follows: eight azimuthal solid angle segments cover the equatorial band between ±22.5°(containing measurements from instrument pixels PF4, PF5, PF12, and PF13), and four azimuthal segments each cover the spin and antispin quadrants for polar angles from 22.5° to 90° (PF1-PF3 and PF14-PF16) and -22.5° to -90°(PF6-PF11) respectively (see Figure 3b). Hi-mass data are contained in APID 1028 (hex 404).

5.1.5 PHA Events Data

This science data product contains detailed information on a sample of individual pulse height events as collected by the instrument. Besides providing full resolution data, the main purpose of this product is to monitor the resolution and background performance of the sensor. This is necessary to keep the mass selection criteria used for the science data products optimized throughout the mission. The number of events collected per spin depends on the TEAMS mode, and varies from 128 to 2048 events/spin. A threshold can be set to eliminate events at low times-of-flight (e.g. to eliminate protons in order to concentrate on less abundant species). The events thrown out are counted and telemetered. Each event uses 32 bits and contains the following information shown in Table I.

A scheme has been devised to ensure that accumulated PHA events contain a sampling of different angles and energy steps. During each spin, one energy step is selected, and N events are collected for that step, for each sweep in the spin. During the next spin, the selected energy step number is incremented by 4. Thus after 16 spins, the full energy range has been covered. If the rates are low, so that N events are not collected in the selected step, events will continue to accumulate in subsequent steps. The number N varies with mode from 4 to 32. PHA data are contained in APID 1031 (hex 407).

TABLE I

PHA events data structure

Name	Byte#	Bits	Description
TOF	1	0-7	Time-of-flight channel number (0-255)
Start Position	2	0-7	One bit for each start pixel
Energy Step	3	0-7	Microstep number (0-191)
Spin Angle	4	0-5	Angle 0-63
Section	4	6	Instrument half (0=>PF1-8(HS); 1=>PF9-16(LS)
Stop Position	4	7	1 if one stop pixel triggered, 0 if both triggered

5.1.6 Monitor Rates Data

This data quantity provides insight into the sensor efficiency and the operation of the analog and event selection electronics on a continuous basis. All spacecraft telemetry modes contain this product. These data are used to monitor a sampling of events as they occur on each start pixel, each stop quadrant, and to monitor valid and non-valid events. Singles rates provide a measure of the instrument background due to penetrating radiation. During nominal operation the ratios of the coincidence and singles rates data provide a measure of the instrument start-stop efficiencies and of microchannel plate gains. In in-flight calibration mode they provide a health check of the event selection logic. As with the PHA data, only one energy step is measured per spin, and the selected energy step increments by four at the start of each spin. The subcommutation scheme is identical to that used for the PHA data. Rates data are contained in APID 1030 (hex 406).

5.1.7 Status Data

This data product contains an image of the actual command settings of the sensor. Status data are contained in APID 1059 (hex 423).

5.1.8 Housekeeping Data

The housekeeping is comprised of all high voltage supply voltages and supply currents, the internal + and - 5 and 12 V voltages, as well as the temperature at the MCPs, in the time-of-flight electronics, on the postacceleration HV supply and in the digital electronics. These values are read by the IDPU, and come out in the IDPU telemetry data products.

5.2 OPERATING MODES

There are ten basic science telemetry modes producing instrument bit rates from 7.8 kbps to 315 kbps. Three additional engineering modes are defined. Table II shows the output frequency of each of the TEAMS science data products as a function of science mode. The mode nomenclature in the top line of Table II refers to two Slow Survey (SS) Modes (modes 0 and 1), six Fast Survey (FS) modes, and two Burst (Bst) Modes. When the spacecraft is in a “Burst” mode, the burst data is telemetered in addition to the data from one of the Fast Survey modes.

6. Test and Calibration Results

A compilation of time-of-flight spectra for the key ion species at about 20 keV/charge total energy (incoming energy plus energy added by post-acceleration) is shown in Figure 4a. This is the resolution achieved at low energies when the post-acceleration is operating near -20 kV. Because the major species in the magnetosphere are separated by factors of 2 in mass/charge a

TABLE II

TEAMS telemetry modes chart

Output frequency (in spins) of each data product versus telemetry mode

Mode Name Mode Number	SS-2 (0)	SS-1 (1)	FS-1 (2)	FS-1a (3)	FS-2 (4)	FS-2a (5)	FS-3 (6)	FS-3a (7)	Bst-B (8)	Bst-A (9)
# Sweeps/spin	32	32	64	32	64	32	64	32	64	32
Survey—H^+, O^+	2	4	2	2	1	1	.5	.5		
Survey—He^{++}, He^+	4	8	4	4	2	2	1	1		
Hi Mass	16	16	16	16	8	8	4	4		
Pole—H^+, O^+	-		0.016	0.031	0.016	0.031	0.016	0.031		
Pole—He^+, He^{++}	-						0.016	0.031		
Burst									0.016	0.031
Rates	0.031	0.031	0.016	0.031	0.016	0.031	0.016	0.031		
PHA*	128	128	512	256	1024	512	2048	1024		
Status	1	1	1	1	1	1	1	1	1	1

*PHA is shown as # of events per spin

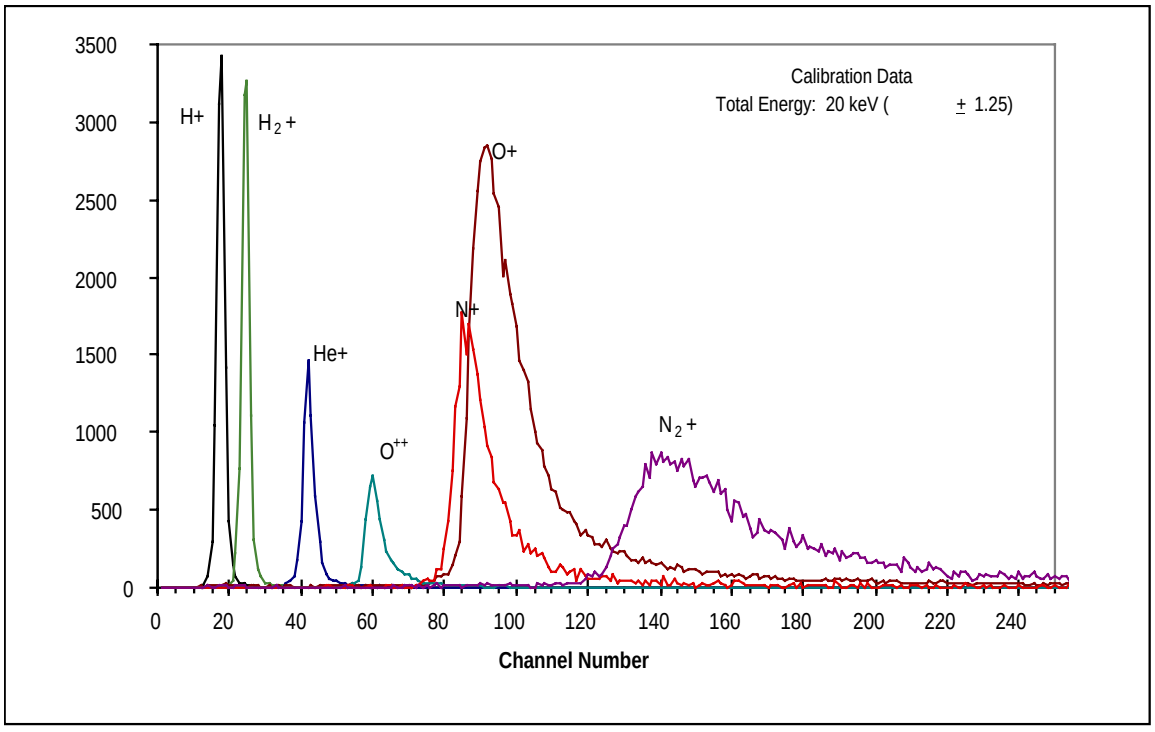

Fig. 4a. Example of a time-of-flight spectrum from calibration data.

clear identification of these ions is possible. As can also be seen, ions with close masses such as N^+ and O^+ cannot be easily distinguished. The peak at mass per charge 2 AMU/e (He^{++} or H_2^+) occurs at time-of-flight values where the H^+ counts have dropped to 1% of their peak value. Therefore He^{++} abundances of 1% are difficult to distinguish, but higher abundances can be measured. Figure 4b shows an example of the time-of-flight spectrum measured during a pass over the aurora. The H^+ peak has been truncated at 1000 counts in order to better show the heavy ion peaks. The post-acceleration is operating at -19.7 kV at this time, and counts from energies up to 1 keV incoming have been included in the figure. The peaks are wider than in Figure 4a because the accelerator beams are monoenergetic while the flight peaks reflect both the acceptance energy width of the electrostatic analyzer, and the 1 kV band included in the figure to increase statistics. The O^+ flight peak is at higher times-of-flight because the calibration data point is for 21 keV total energy, while the flight O^+ is dominiated by ions close to 19.7 keV. It can be seen that the goal of separating the major species has been met with the present design.

While the response of an ESA remains essentially unchanged for different species and over the entire energy range, the detection efficiency of TOF assemblies changes with species and energy due to dependencies of the secondary electron production and the sensitivity of the MCPs. To reduce the anticipated variations the MCPs are operated in saturation of their gain. Yet there are still significant variations of the efficiency with species, energy, and position on the MCPs that may be as large as a factor of 2. Therefore, the sensor has been calibrated in a matrix of ion species, energies and MCP position. The final calibration was performed using the University of Bern ion beam test and calibration facility. A monoenergetic ion beam of known flux is directed at the instrument. The collimated beam fully illuminates the entrance aperture. The ratio of the instrument output to the known input is then used to determine the overall efficiency. Figure 5a-c shows the efficiencies for each of the three species, H^+, He^+, and O^+, as a function of energy in each of the 16 positions on the sensor. For He^+ and O^+, an average curve is also shown. This curve is based on measurements with the Cluster CODIF instrument, which covered a larger energy range. For these species, the average curve fit the individual curves well, except for an overall normalization factor. For H^+, a few of the positions were significantly different, so individual fits to the pixels were used for the final calibration factors. The efficiency for He^{++} is the same as the efficiency for He^+ at the same total energy.

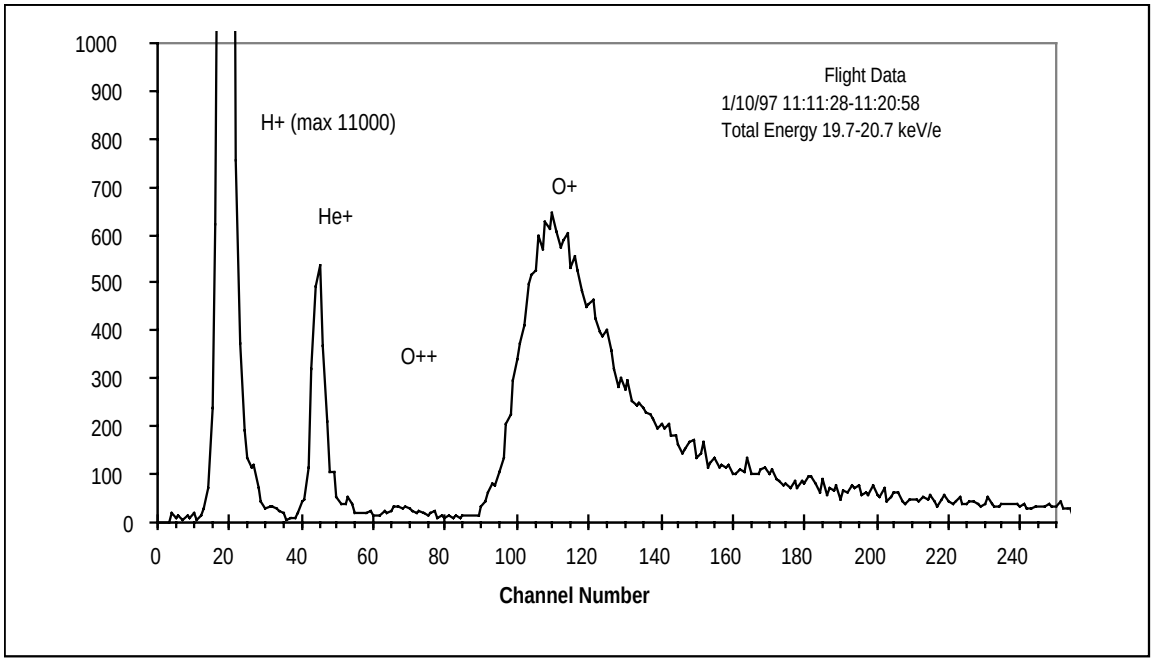

Fig. 4b. Example of a time-of-flight spectrum for TEAMS operating in flight.

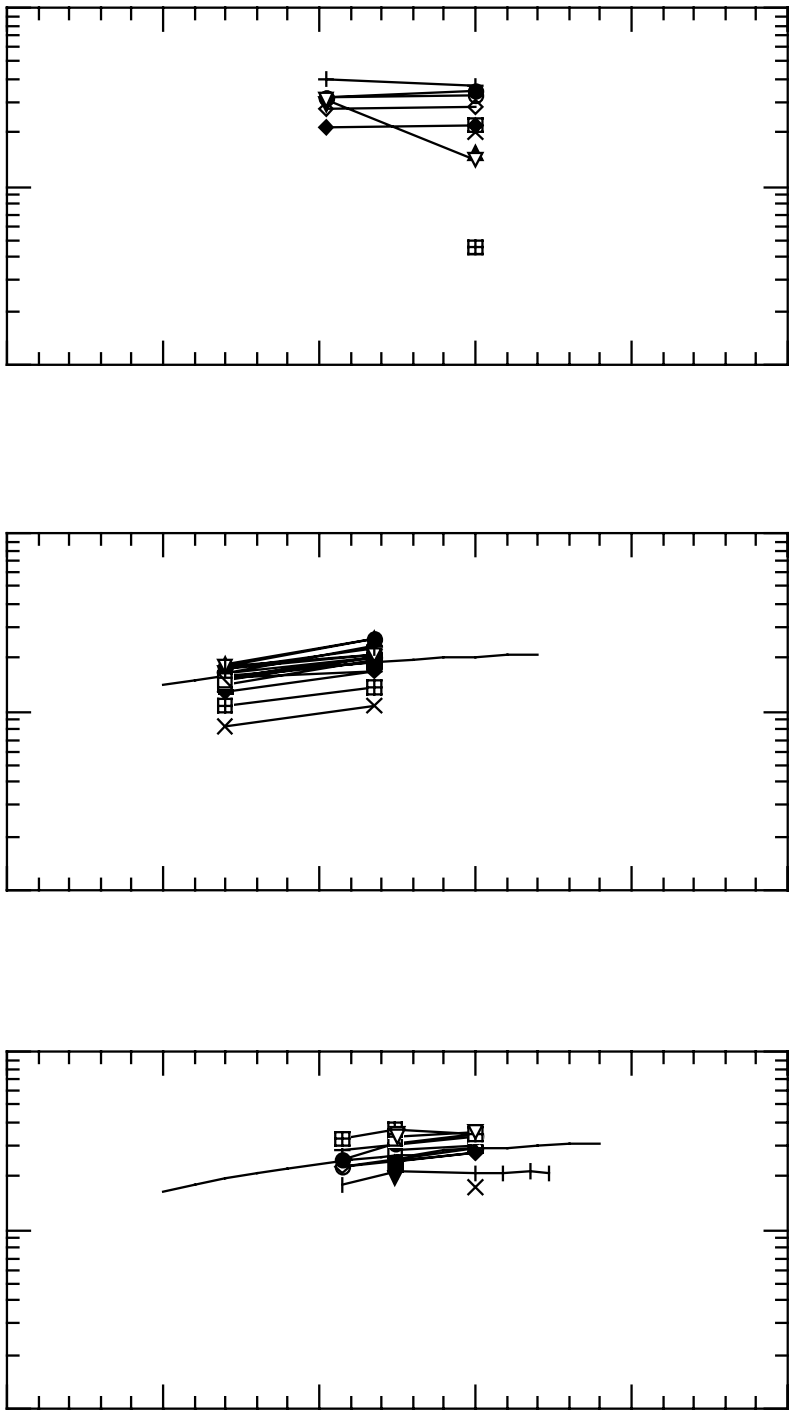

Fig. 5. Total efficiencies for the species H^+, He^+, and O^+ as a function of energy.

Figure 6 shows the acceptance region of the sensor in electrostatic analyzer voltage and azimuthal angle (in the direction of the ESA deflection). The overall acceptance region is typical for this type of ESA. One deviation from the norm is the two-ridge structure, with the valley in between. Normally, just one ridge is observed. This feature is due to the fact that the incoming ion beam is focused by the post-acceleration field at the TOF entrance, and the resulting beam is

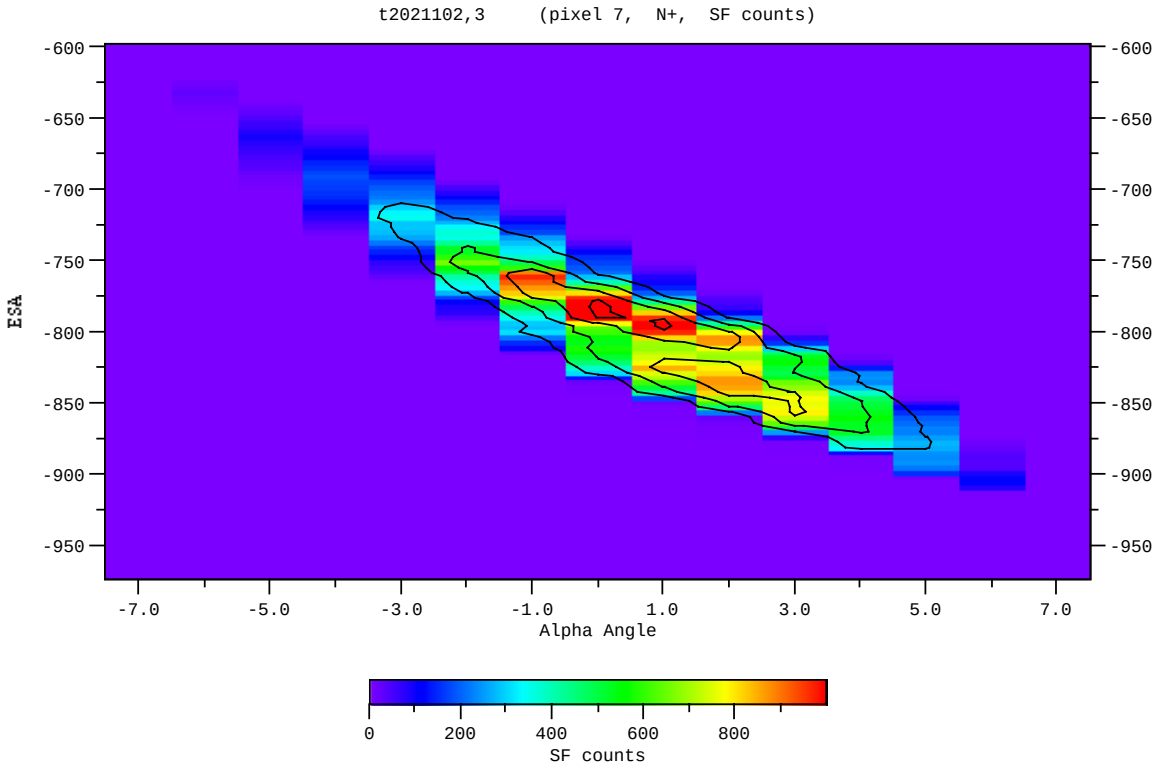

Fig. 6. Example of the response of the sensor in energy and elevation angle.

so narrow that the carbon foil support grid structure becomes visible. The variation of the response as a function of ESA voltage (in a) and azimuthal angle (in b) is shown in Figure 7. In both cases the response has been integrated over azimuthal angle (in a) and ESA voltage (in b), respectively. Except for the small minimum observed at the peak in a), the curves closely match the theoretical response of the ESA. The remaining effect of the carbon foil support grids is a reduction of the detected flux according to the transmission factor of the grids, which is included in the overall geometric factor.

7. In-Flight Performance

Figure 8 shows an overview of FAST plasma measurements including the TEAMS ion composition results during a typical auroral pass in the northern hemisphere for January 23, 1997, at about 4100 km in the premidnight magnetic local time sector. Shown for a 4-minute interval are from top to bottom: the electron ESA energy-time (E-t) spectrogram for 5 - 30000 eV, averaged over all pitch-angles; the TEAMS H^+ E-t spectrogram (0-360° pitch angle), the TEAMS H^+ E-t spectrogram for the pitch angle subset 150° to 210°; O^+; and He^+ spin-averaged E-t spectrogram for 1 - 12000 eV; and the pitch-angle vs time spectrogram for ions measured by the ion ESA without mass discrimination. The four ion composition panels are produced from the four angle sectors adjacent to the spin plane using the TEAMS survey data set. The Fast-Survey mode in use at this time produces half-spin resolution data for hydrogen and oxygen and one-spin resolution data for the helium ions.

Four distinct upflowing ion beam events are present during the period shown, most clearly delineated by the intense flux covering a few degrees in pitch angle at 180° as illustrated by the red horizontal stripes in the lower panel beginning at 1004:55, 1005:50, 1006:10, and 1006:50 UT. The strong ion beams with energies up to several keV are observed along with the

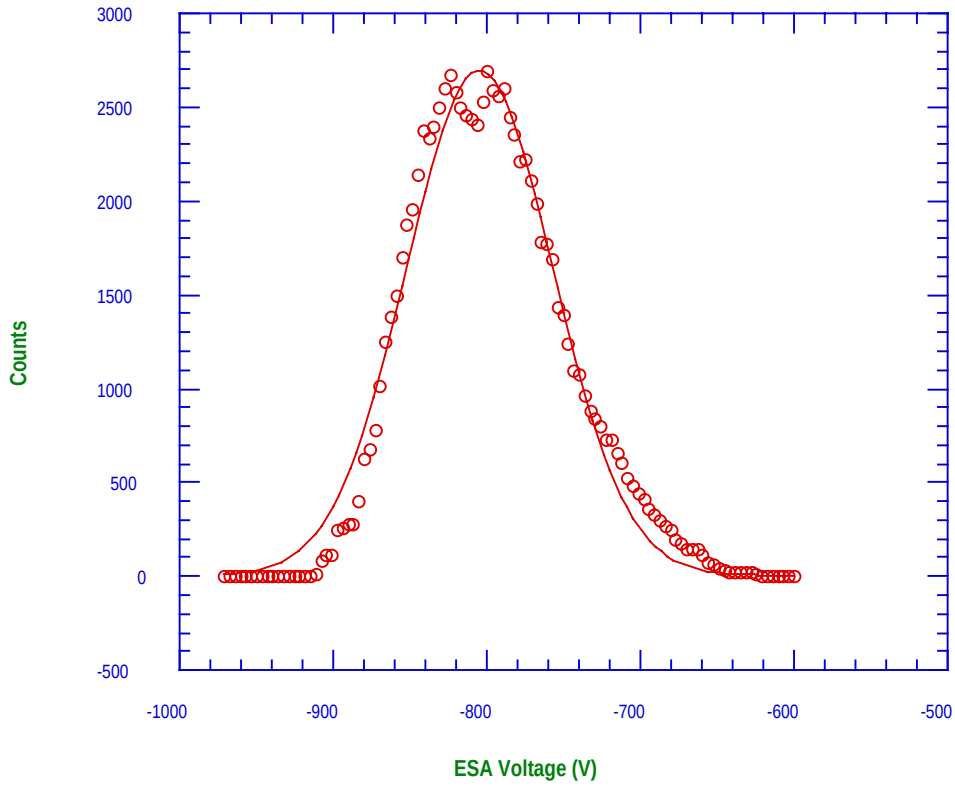

Fig. 7a. Response of instrument integrated over azimuthal angle.

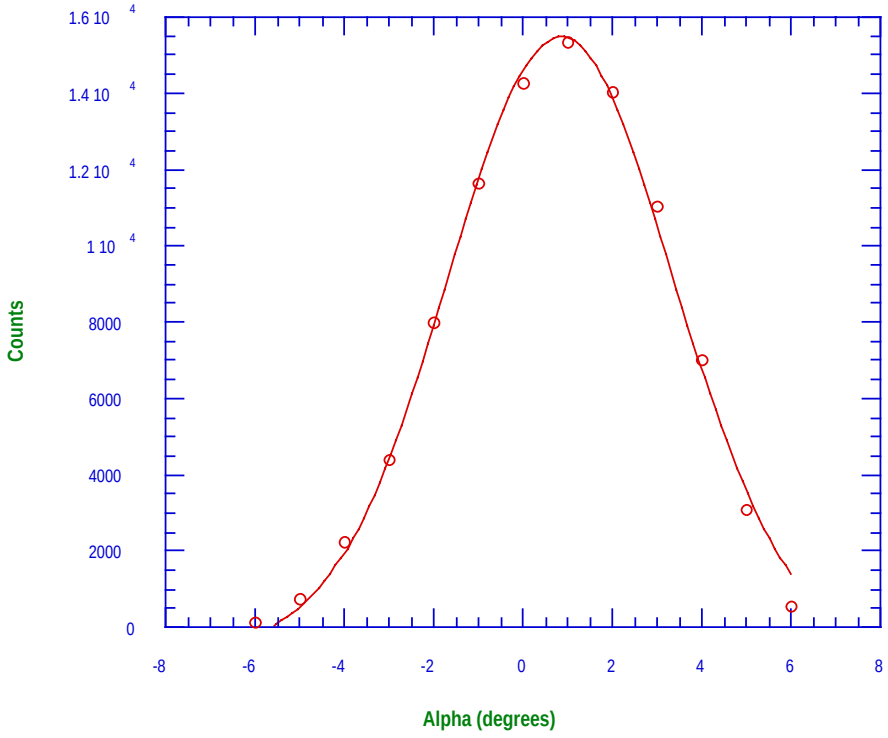

Fig. 7b. Response of instrument integrated over energy.

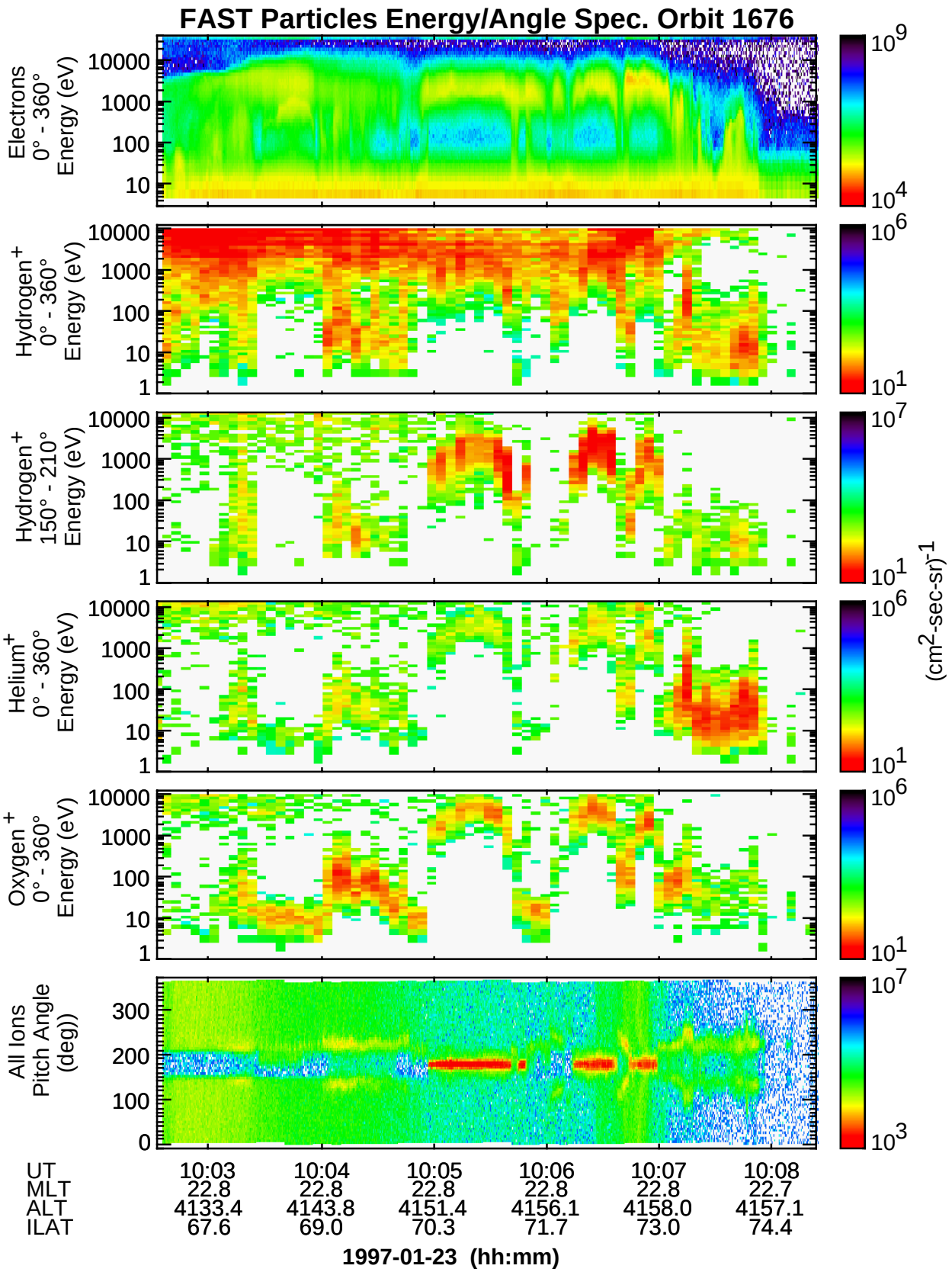

Fig. 8 Overview of FAST plasma measurements.

occurrence of electron cavities (indicated by the reduction of electron flux below 1000 keV in the top panel). The hydrogen in the upflowing beams is most clearly discerned by selecting only upward moving ions, as was done in the third panel, thereby excluding ions precipitating out of the magnetosphere. The precipitating ions are clearly present in panel two, where they have not been excluded, at energies above about 1 keV The ion beams consist of H^+, He^+ and O^+ with varying relative abundances and with peak energies that systematically vary with mass. A study of these mass dependent ion beam variations is contained in Möbius et al. (1998a).

Also present in these data are ions whose pitch angle distributions peak near, or just above, the edge of the loss cone. These distributions, known as Transverseley Accelerated Ions, or "Conics," are indicated in the bottom panel by the less distinct (and less intense) yellow shades centered about 40° away from 180° pitch angle beginning at 1004:00, 1006:05, 1006:40, and 1007 UT. These ions are also being accelerated out of the ionsophere, but through a distinctly different process than the one that acts to form the ion beams. As the E-t spectrograms show typical ion energies are lower in these distributions than in the ion beams.

Acknowledgements

The instrument team is indebted to the many unnamed individuals in the electronic and machine shops as well as administrative and support units, at all institutions involved in the hardware development and implementation of the instrument. The development, fabrication and test of the instrument is being supported by NASA under contract #NAS5-31283. Calibrations at the Bern calibration facility were supported by the Swiss National Science Foundation.

References

Carlson, C. W., J. P. McFadden, P. Turin, D. W. Curtis, and A. Magoncelli: 2000, 'The electron and ion plasma instrument on FAST', *Space Sci. Rev.*,this issue.

Carlson, C. W. and J. P. McFadden: 1998, 'Design and application of imaging plasma instruments', *Measurement Techniques in Space Plasmas*, American Geophysical Union, *Geophys. Monog.*, **102**, 125-140.

Carlson, C.W., The Fast Auroral Snapshot Explorer: June 9, 1992, *EOS*, **73**, no. 23, pp 249.

Carlson, C. W., D. W. Curtis, G. Paschmann, and W. Michael: 1982, 'An instrument for rapidly measuring plasma distribution functions with high resolution', Adv. Space Res., **2**, no. 7, pp 67.

Ghielmetti, A. G. and D. T. Young: 1987, 'A double-focusing toroidal mass spectrograph for energetic plasmas, I, theory', *Nucl. Instr. Meth.*, **A258**, pp 297.

Gloeckler, G., F. M. Ipavich, W. Studemann, B. Wilken, D. C. Hamilton, G. Kremser, D. Hovestadt, F. Gliem, R. A. Lundgren, W. Rieck, E. O. Tums, J. C. Cain, L. S. MaSung, W. Weiss, and P. Winterhof: 1985, 'The charge-energy-mass spectrometer for 0.3 - 300 keV/e ions on the AMPTE/CCE', *IEEE Trans. on Geosci. and Remote Sens.*, **GE-23**, pp 234-240.

Hamilton, D.C., G. Gloeckler, F. M. Ipavich, R. A. Lundgren, R. B. Sheldon, and D. Hovestadt: 1990, 'New-High Resolution Electrostatic Ion Mass Analyzer Using Time-of-Flight', *Rev. Sci. Instrum.*, **61**, pp 3104-3106.

Hovestadt, D., et al.: 1989, 'CELIAS - Charge, Element and Isotope Analysis System for SOHO', *The SOHO Mission*, **ESA SP-1104**, pp 69, Noordwijk, The Netherlands.

Klumpar, D. M.: 1979, Transverseley accelerated ions: An ionospheric source of hot magnetospheric ions, *J. Geophys. Res.*, **84**, pp 4229.

McComas, D.J. and J.E. Nordholt: 1990, 'New approach to 3-D, high sensitivity, high mass resolution space plasma composition measurements', *Rev. Sci. Instrum.*, **61**, pp 3095-3097.

McEntire, R.W., E.P. Keath, D.E. Fort, A.T.Y. Lui, and S.M. Krimigis: 1985, 'The Medium-Energy Particle Analyzer (MEPA) on the AMPTE CCE spacecraft', *IEEE Trans. on Geosci. and Remote Sens.,* **GE-23**, pp 230-233.

Möbius, E., L. Tang, L. M. Kistler, M. Popecki, E. J. Lund, D. M. Klumpar, W. Peterson, E. G. Shelley, B. Klecker, D. Hovestadt, C. W. Carlson, R. Ergun, J. P. McFadden, F. Mozer, M. Temerin, C. Cattell, R. Elphic, R. Strangeway, and R. Pfaff: 1998a, 'Species dependent energies in upward directed ion beams over auroral arcs as observed with FAST TEAMS', *Geophys. Res. Lett.*, **25**, pp 2029-2032.

Möbius, E., L. M. Kistler, M. A. Popecki, K. N. Crocker, M. Granoff, Y. Jiang, E. Satori, V. Ye, H, Rème, J. A. Sauvaud, A. Cros, C. Aoustin, T. Camus, J. -L. Médale, J. Rouzaud, C. W. Carlson, J. P. McFadden, D. Curtis, H. Heetdirks, J. Croyle, C. Ingraham, B. Klecker, D. Hovestadt, M. Ertl, F. Eberl, H. Kästle, E. Künneth, P. Laeverenz, E. Seidenschwang, E. G. Shelley, D. M. Klumpar, E. Hertzberg, G. K. Parks, M. McCarthy, A. Korth, H. Rosenbauer, B. Gräve, L. Eliasson, S. Olsen, H. Balsiger, U. Schwab, and M. Steinacher: 1998b, 'The 3-D Plasma Distribution Function Analyzers with Time-of-Flight Mass Discrimination for CLUSTER, FAST, and Equator-S', *Measurement Techniques in Space Plasmas*, American Geophysical Union, *Geophys. Monog.*, **102**, pp 243-248.

Möbius, E., P. Bochsler, A.G. Ghielmetti, D.C. Hamilton: 1990, 'High mass resolution isochronous Time-of-flight spectrograph for three-dimensional space plasma measurements', *Rev. Sci. Instrum.,* **61**, pp 3609 - 3612.

Möbius, E., G. Gloeckler, D. Hovestadt, F. M. Ipavich, B. Klecker, M. Scholer, H. Arbinger, H. Höfner, E. Künneth, P. Laeverenz, A. Luhn, E. O. Tums, and H. Waldleben: 1985, 'The time-of-flight spectrometer SULEICA for ions of the energy range 5 - 270 keV/charge on the AMPTE/IRM', *IEEE Trans. on Geosci. and Remote Sens.,* **GE-23**, pp 274-279.

Paschmann, G., H. Loidl, P. Obermayer, M. Ertl, R. Laborenz, N. Sckopke, W. Baumjohann, C. W. Carlson, and D. W. Curtis: 1985, 'The plasma instrument for AMPTE/IRM', *IEEE Trans. on Geosci. and Remote Sens.,* **GE-23**, pp 262-266.

Rème, H., J. A. Bosqued, J. A. Sauvaud, A. Cros, J. Dandouras, C. Aoustin, Ch. Martz, J. L. Médale, J. Rouzaud, E. Möbius, et al.: 1993, 'The Cluster ion spectrometry experiment', **ESA SP-1159**, pp 133-162.

Sharp, R. D., R. G. Johnson, and E. G. Shelley: 1977, 'Obseration of an ion acceleration mechansim producing energetic (keV) ions primarily normal to the geomagnetic field direction', *J. Geophys. Res.*, **82**, pp 3324-3328.

Shelley, E. G., A. G. Ghielmetti, H. Balsiger, R. K. Black, J. A. Bowles, R. P. Bowman, O. Bratschi, J. L. Burch, C. W. Carlson, A. J. Coker, et al: 1995 'The toroidal imaging mass-angle spectrograph (TIMAS) for the Polar mission,' *Space Sci. Rev.,* **71**, pp 497-530.

Shelley, E. G., R. D. Sharp, and R. G. Johnson: 1976, 'Satellite observations of an ionospheric acceleration mechanism', *Geophys. Res. Lett.*, **3**, pp 654-657.

Shelley, E. G., R. G. Johnson, and R. D. Sharp: 1972, 'Satellite observations of energetic heavy ions during a geomagnetic storm', *J. Geophys. Res.*, **77**, pp 6104-6110.

Young, D. T., S. J. Bame, M. F. Thomsen, R. H. Martin, J. L. Burch, J. A. Marshall, and B. Reinhard: 1988, '2-pi-radian field-of-view toroidal electrostatic analyzer', *Rev. Sci. Instr*, **59**, pp 743-751.

Young, D. T., J. Geiss, H. Balsiger, P. Eberhardt, A. Ghielmetti, and H. Rosenbauer: 1977, 'Discovery of He^{2+} and O^{2+} ions of terrestrial origin in the outer magnetosphere', *Geophys. Res. Lett.*, **4**, pp 561-564